Supplemental Material

Neuron, 68(5), 921–935, Dec. 2010.

Calcium store depletion induces persistent perisomatic increases in the functional density of *h* channels in hippocampal pyramidal neurons

Rishikesh Narayanan, Kevin Dougherty and Daniel Johnston

Center for Learning and Memory,
The University of Texas at Austin, Austin, TX 78712

Supplemental Figure S1 2
Supplemental Figure S2 3
Supplemental Figure S3 4
Supplemental Figure S4 5
Supplemental Figure S5 6
Supplemental Figure S6 7
Supplemental Figure S7 9
Supplemental Figure S8 11
Supplemental experimental procedures 12
Supplemental references 15

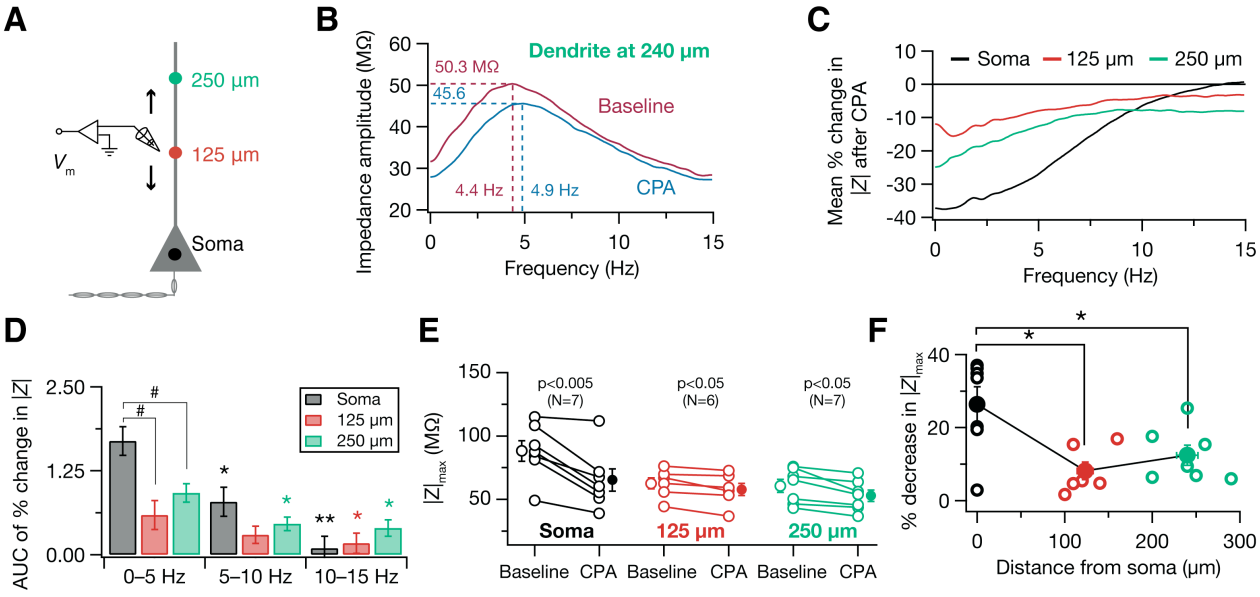

Figure S1. Depletion-induced plasticity was predominantly in the lower frequency and was accompanied by a reduction in maximal impedance amplitude. (A) Experimental setup for CPA treatment. Details are the same as Figure 1A. (B) Impedance amplitude profiles (ZAP) of a dendrite, located at 240 *µ*m from the soma, computed during the baseline period and 40 min after CPA treatment. (C) Average percentage change in |*Z*| obtained for each of the three subpopulations (Soma, 125 *µ*m and 250 *µ*m) plotted as functions of frequency. This was computed by dividing ZAP obtained after CPA treatment by the corresponding ZAP during baseline for each somatic and dendritic recording, converting this ratio to percentage change, and averaging these percentages over all recordings within the three subpopulations (D) To quantify the average percentage change in |*Z*| as a function of frequency, we split the analyzed frequency range (0–15 Hz) to three 5 Hz groups, and measured the area under the curves (AUCs) shown in (C) for each of the three subpopulations. For all three subpopulations, the amount of changes in higher frequencies was significantly lower than those at lower frequencies. Color-coded asterisk (*) above a group represents that the values within that group were significantly different compared with the values in the 0–5 Hz group of the same subpopulation (*Friedman's* nonparametric repeated measures ANOVA test followed by *Dunn's* multiple comparison test; *: p <0.05; **: p<0.001). In all three subpopulations, the values in the 5–10 Hz group were not significantly different from those in the 10–15 Hz range (*Friedman's* nonparametric repeated measures ANOVA test, p>0.05). Across subpopulations, within each of the three frequency ranges, values were significantly different only in the 0–5 Hz group (#: p<0.05, *Kruskal-Wallis* test). (E) Population plots of maximal impedance amplitude ($|Z|_{max}$) measured before (baseline; open circles) and 40 min after CPA wash in (CPA; solid circles) show significant reductions in $|Z|_{max}$ (paired *Student's t* test) after CPA treatment, in all three subpopulations. (F) Scatterplot of data in (E). Each open circle represents the percentage of reduction, 40 min after CPA treatment, relative to the respective baseline value of $|Z|_{max}$ in a given experiment. The solid circles represent the average distance and average plasticity for the three subpopulations. *: p<0.05; *Kruskal–Wallis* test followed by *Dunn's* test.

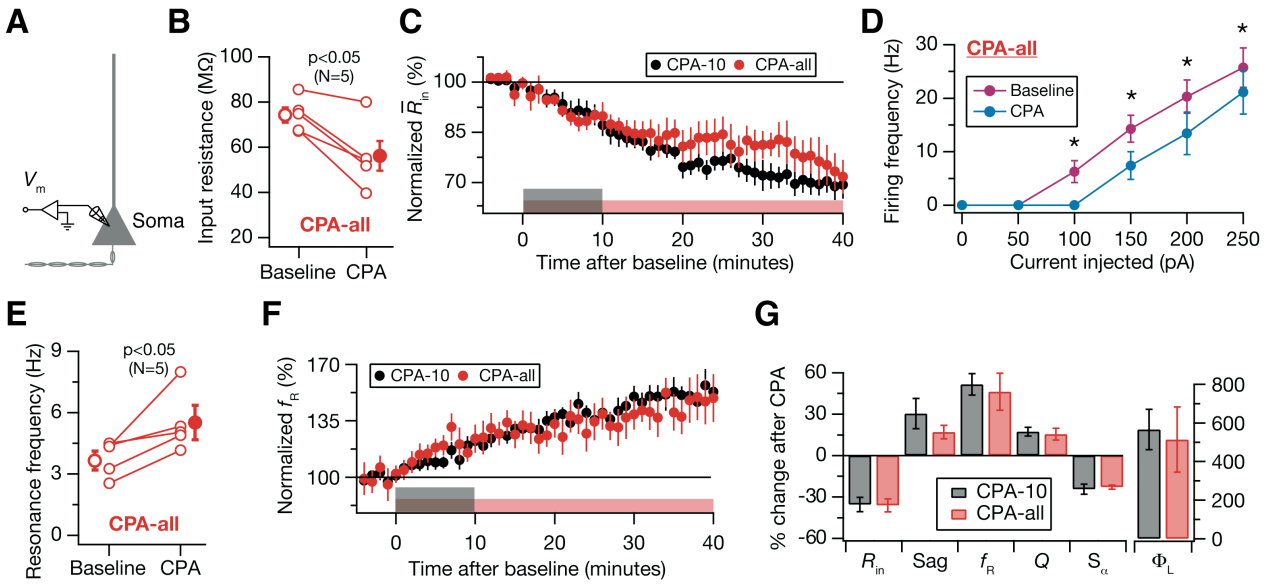

Figure S2. Depletion-induced plasticity in intrinsic excitability and resonance properties was induced at wash in and not at wash out of CPA. (A) Schematic of the somato-apical trunk depicting the experimental setup. Voltage responses (V_m) of the soma to various current stimuli were recorded using a whole-cell patch-clamp electrode. (B) Population plots of input resistance measured before (Baseline; open circles) and 40 mins of CPA treatment (CPA; solid circles) show a significant reduction (paired *Student's t* test; Baseline: 74 ± 3 MΩ, CPA: 56 ± 6 MΩ) after 40 mins of CPA treatment. (C) Time courses of normalized $\overline{R}_{in}$ during CPA treatment experiments show that the reduction in $\overline{R}_{in}$ obtained with 10-min treatment of CPA (black) was not significantly different from the reduction in $\overline{R}_{in}$ obtained with CPA treatment through the course of the experiment (red). Black and red patches in (C) and (F) are color-coded in accordance with the corresponding group's marker color, and represent CPA treatment periods. (D) Population plots of action potential firing frequency as a function of injected current to the soma establish significant reductions 40 mins of CPA treatment (Baseline: magenta; 40 min after CPA: cyan). *: $p<0.05$, paired *Student's t* test. (E) Population plots of f_R measured before (Baseline; open circles) and 40 mins of CPA treatment (CPA; solid circles) show a significant increase in resonance frequency (paired *Student's t* test; Baseline: 3.65 ± 0.46 Hz, CPA: 5.52 ± 0.84 Hz) after 40 mins of CPA treatment. (F) Time courses of normalized f_R during CPA treatment experiments show the increase in f_R obtained with 10-min treatment of CPA (black) is not significantly different from the increase in f_R obtained with CPA treatment through the course of the experiment (red). (G) Summary plot of percentage changes in various measurements sensitive to the *h* current, obtained with 10-min treatment of CPA (CPA–10) and with CPA treatment through the course of the experiment (CPA–all), measured at 40 mins after CPA wash in relative to respective baseline values. After CPA, within the respective group, all measurements were significantly different from their respective baseline values ($p<0.05$; paired *Student's t* test), while none of the measurements had their percentage changes significantly different across the two groups ($p>0.2$; *Mann-Whitney* test).

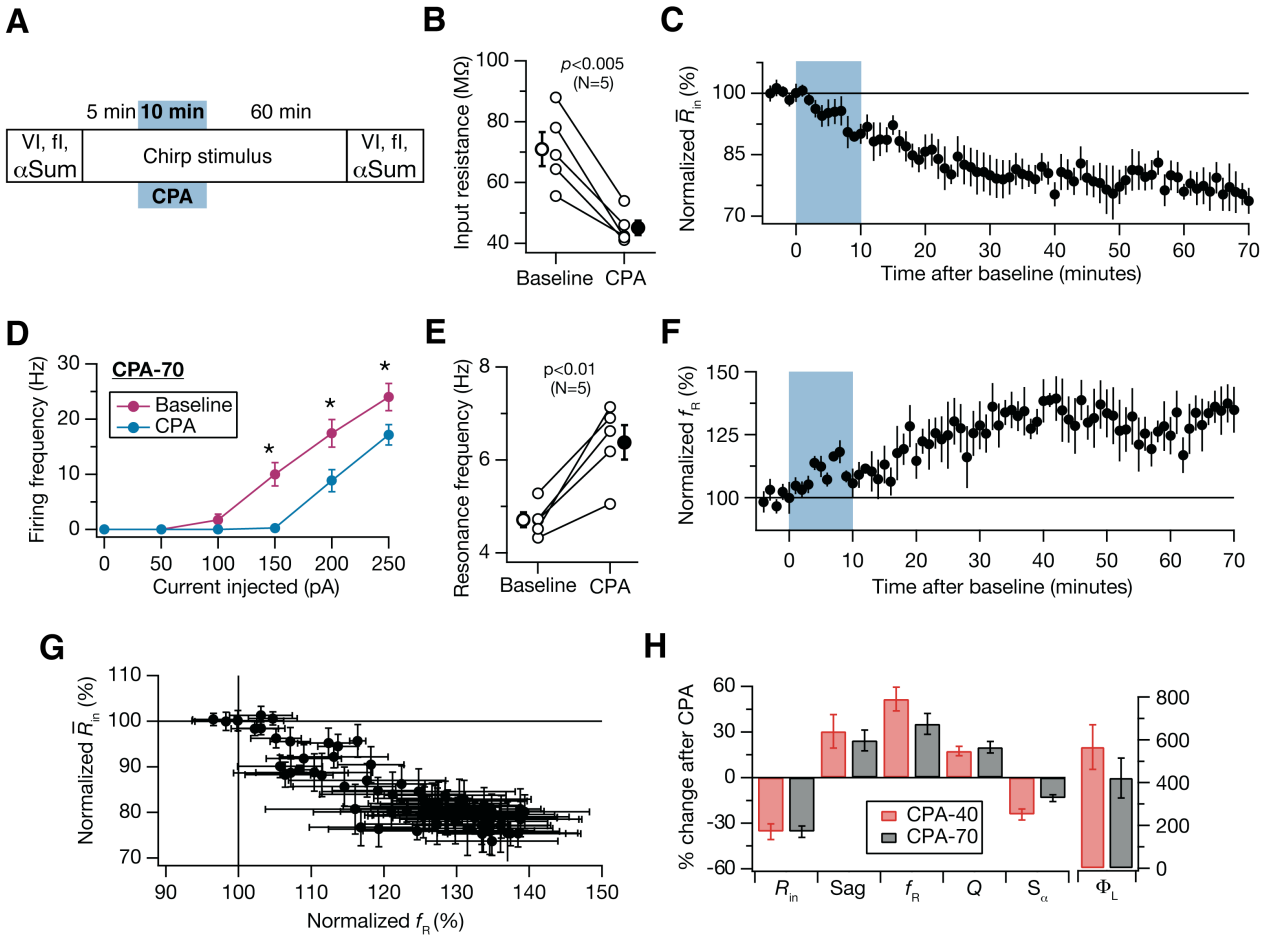

Figure S3. Depletion-induced plasticity in intrinsic excitability and resonance properties lasted at least for 70 mins after CPA wash in. (A) Diagram depicting the experimental protocol for assessing the time extent of depletion-induced plasticity. The protocol is similar to Fig. 1A, except that responses to the *Chirp15* stimulus were continuously recorded for until 70 mins after CPA wash in instead of 40 mins in Fig. 1A. The blue patches represent CPA treatment period. (B) Population plots of R_{in} measured before (Baseline; open circles) and 70 mins after CPA wash in (CPA; solid circles) show a significant reduction (paired *Student's t* test; Baseline: 71 ± 5 MΩ, CPA: 45 ± 2 MΩ) 70 mins after CPA wash in. (C) Time courses of normalized $\bar{R}_{in}$ during CPA treatment experiments show a reduction in input resistance 70 mins following CPA wash in. (D) Population plots of action potential firing frequency as a function of injected current to the soma establish significant reductions 70 mins after CPA wash in (Baseline: magenta; 70 min after CPA: cyan). *: $p<0.05$, paired *Student's t* test. (E) Population plots of f_R measured before (Baseline; open circles) and 70 mins after CPA wash in (CPA; solid circles) show a significant increase in resonance frequency (paired *Student's t* test; Baseline: 4.71 ± 0.16 Hz, CPA: 6.37 ± 0.36 Hz) after CPA wash in. (F) Time courses of normalized f_R during CPA treatment experiments show an increase in f_R 70 mins following CPA wash in. (G) Relationship between changes in f_R and $\bar{R}_{in}$ during CPA treatment experiments establish the correlations between these two measurements. R=–0.88 with *Pearson's* correlation test. (H) Summary plot of percentage changes in various measurements sensitive to the *h* current, at 40 (CPA–40) and 70 (CPA–70) mins after CPA wash in, relative to respective baseline values. After CPA, within the respective group, all measurements were significantly different from their respective baseline values ($p<0.05$; paired *Student's t* test), while none of the measurements had their percentage changes significantly different across the two groups ($p>0.1$; *Mann-Whitney* test).

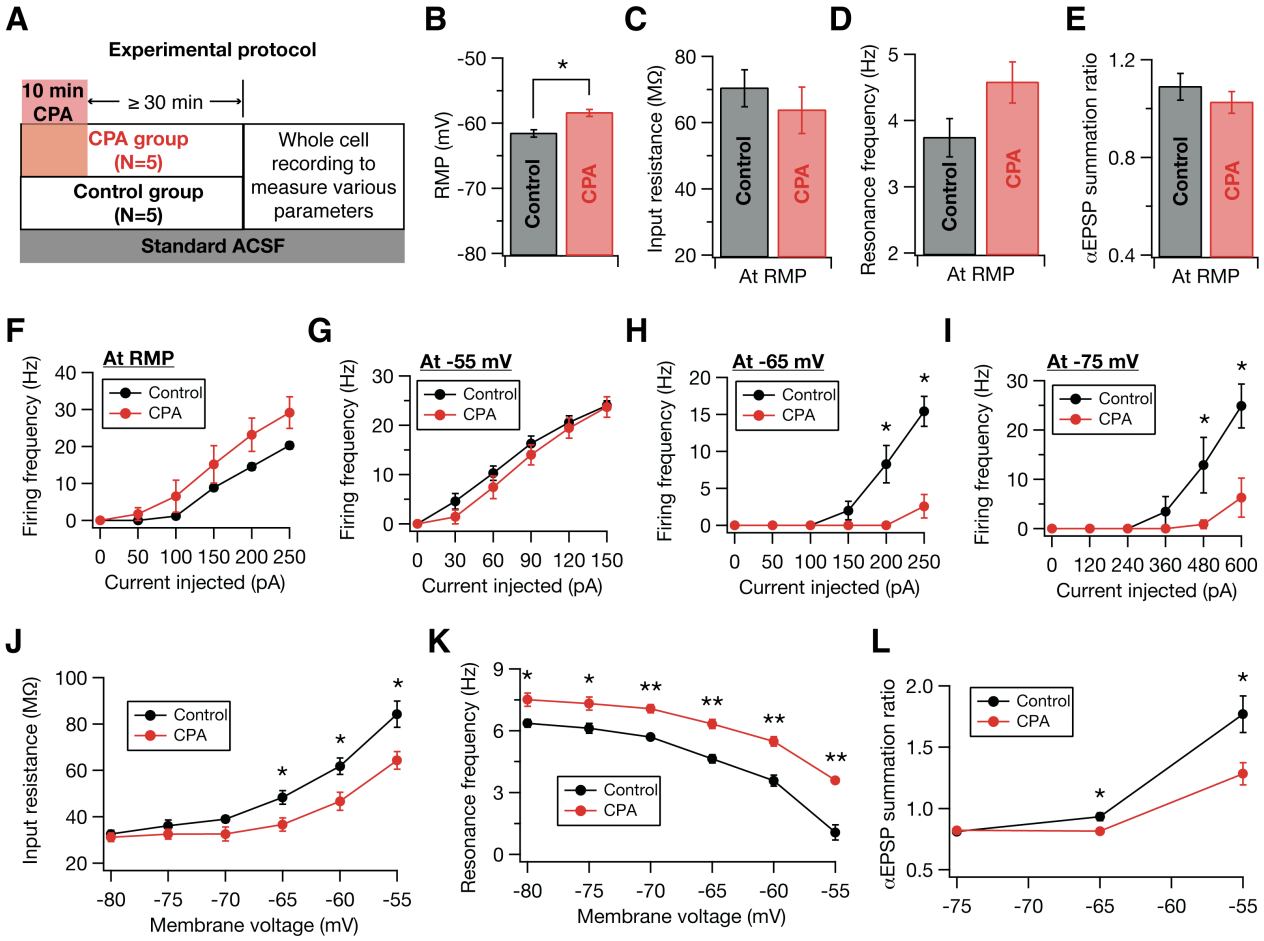

Figure S4. Depletion-induced plasticity in intrinsic excitability and resonance properties expressed even when CPA treatment preceded whole-cell recordings. (A) Experimental protocol for assessing the dependence of depletion-induced plasticity on pipette solution and the patching process. For the CPA group, 20 μM CPA was perfused through the recording chamber containing the slice for 10 mins, and was followed by at least 30 min waiting period during which standard ACSF was perfused. Whole cell recordings were performed after this period with standard ACSF in the recording solution. For the control group, whole cell recordings were performed after perfusing standard ACSF for at least 40 mins, with standard ACSF in the recording solution. (B) The resting membrane potential (RMP) was significantly depolarized in the CPA group (red; -61.6 ± 0.55 mV) in comparison to the Control group (black; -58.4 ± 0.53 mV; $p<0.05$, paired *Student's t* test). Input resistance (C), resonance frequency (D), temporal summation ratio of αEPSPs (E) and action potential firing frequencies for multiple current injections (F) were not significantly different (paired *Student's t* test) across the two groups when measured at their respective RMPs. Action potential firing frequencies were significantly different for multiple current injections across the two groups when measured at –65 mV (H) and –75 mV (I), but not at –55 mV (G). *: $p<0.05$, paired *Student's t* test. (J) When measured at multiple voltages, CPA-treatment significantly reduced input resistance. *: $p<0.05$, paired *Student's t* test. (K) Measured at multiple voltages, CPA-treatment significantly increased resonance frequency at all measured voltages. *: $p<0.05$; **: $p<0.001$, paired *Student's t* test. (L) When measured at multiple voltages, temporal summation ratio of αEPSPs was significantly reduced after CPA treatment. *: $p<0.05$, paired *Student's t* test.

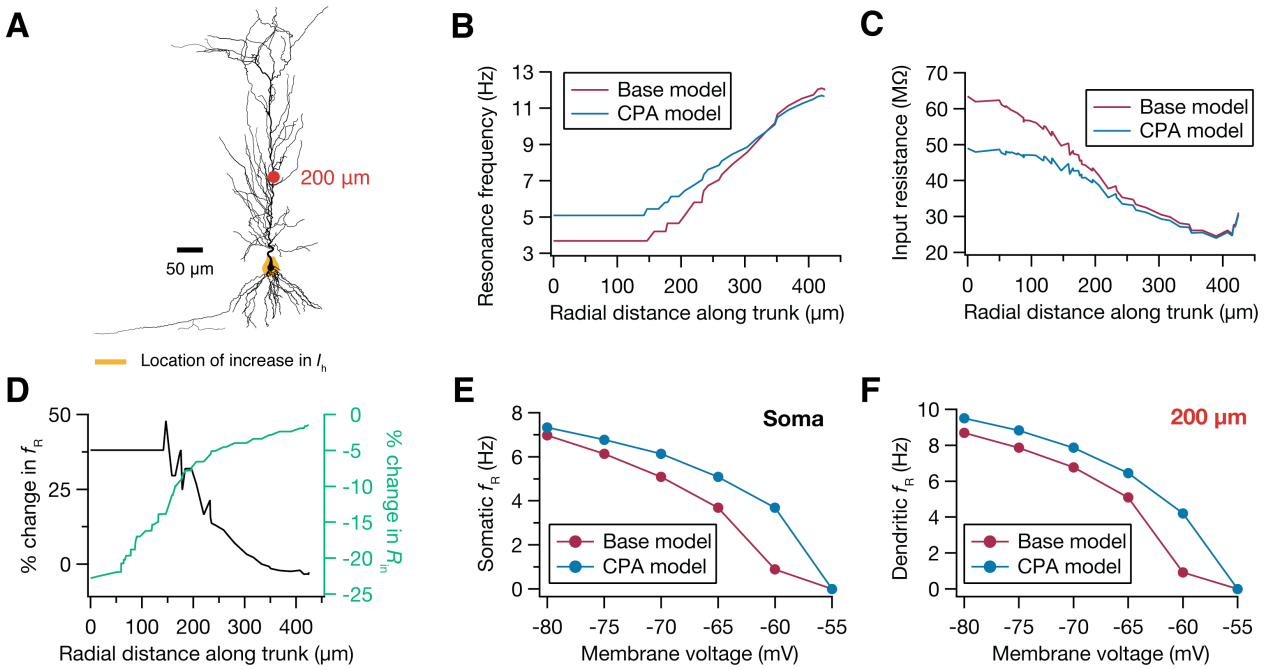

Figure S5. Multicompartmental simulations suggested the requirement for an increase in maximal *h* conductance in conjunction with a depolarizing shift in the *h* channel activation curve for replicating experimental results. (A) Projection of the three-dimensional neuronal reconstruction used for multicompartment simulations, depicting a graphical illustration of location of changes in *h* channel properties (orange shade). The apical trunk location at 200 *µ*m from where the dendritic changes were measured (for F) is marked in red. (B–C) Profiles of local resonance frequency (B) and input resistance (C) along the somato-apical trunk as a function of radial distance from the soma in the model cell, in the base (magenta) and CPA (cyan) models. (D) Percentage changes of resonance frequency (black; f_R) and input resistance (green; R_{in}) in the CPA model in comparison to the base model, as a function of radial distance from the soma. These plots were obtained by finding percentage changes of corresponding measurements in (B) and (C). An increase in local resonance frequency and a concurrent decrease in local input resistance limited largely to the perisomatic compartments may be noted. (E–F) Somatic (E) and dendritic (F; at 200 *µ*m distance from the soma) local resonance frequency as functions of membrane voltage in both the base (magenta) and the CPA (cyan) models. It may be noted that the amount of increase in resonance frequency is much higher at depolarized voltages than at their hyperpolarized counterparts. Further, it may also be noted that the amount of increase in resonance frequency is much higher at the soma than at the dendrites. Compare with Fig. 3 and Fig. 5 to observe the similarity of these simulation outcomes with experimental results.

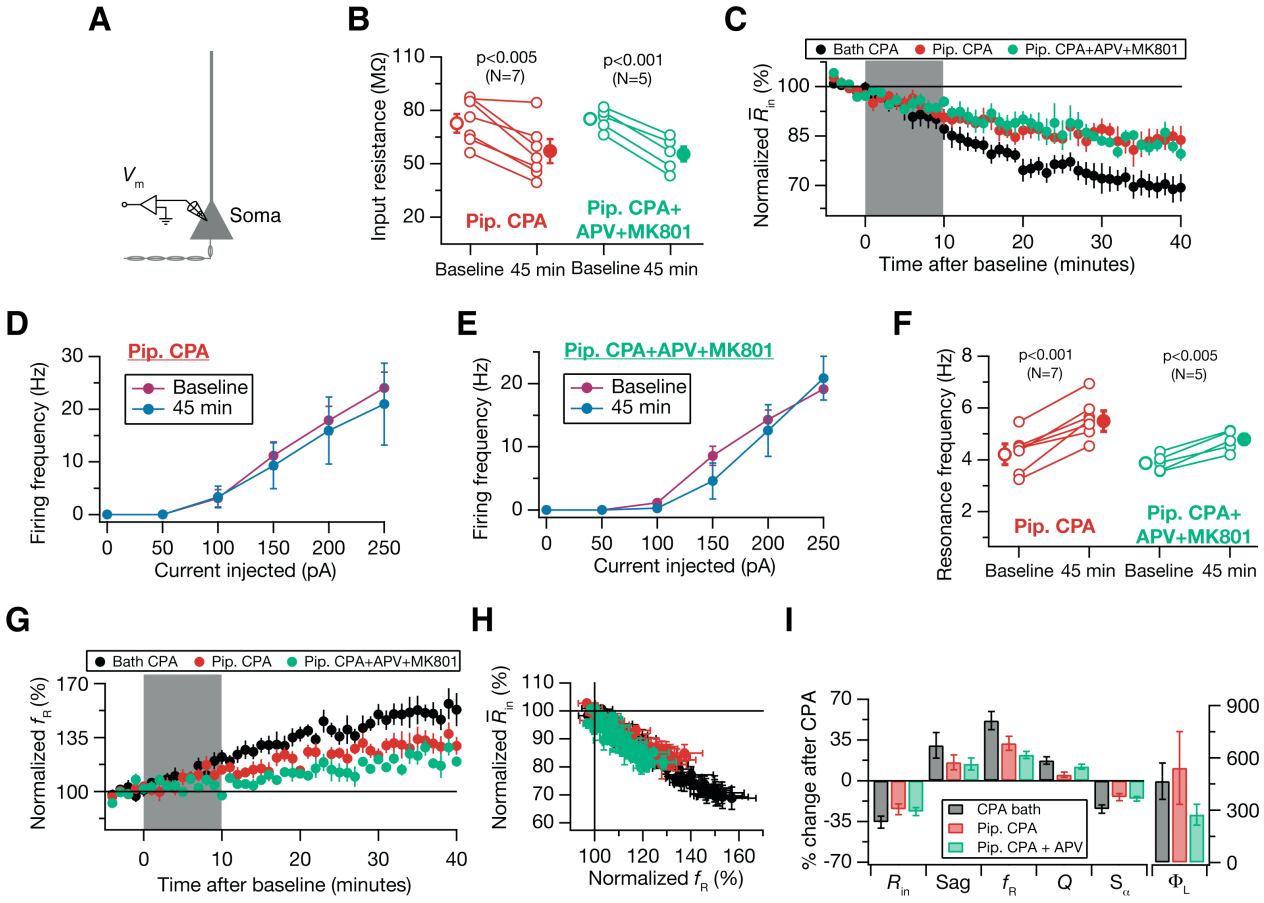

Figure S6. Depletion-induced plasticity in intrinsic excitability and optimal response frequency expressed even when CPA was present only in the recording pipette. (A) Diagram depicting the experimental setup. For all experiments illustrated in this figure, voltage recordings at the soma (V_m) were performed with 20 μM CPA present only in the recording pipette. Experiments were performed with either normal saline (Pip. CPA group) or 50 μM D,L–APV and 10 μM MK801 (Pip. CPA+NMDAR group) in the recording solution. (B) Population plots of R_{in} measured at the beginning of the experiment (Baseline; open circles) and 45 mins later (CPA; solid circles) showing significant reductions (paired *Student's t* test) in experiments performed with standard ACSF in the bath (red), and with NMDAR blockers (green). (C) Time courses of normalized $\overline{R}_{in}$ in experiments performed with CPA in the recording pipette showed significant reductions (red) in input resistance 45 mins after the beginning of the experiment. The amount of reduction was not significantly different even when NMDAR blockers (green), 50 μM D,L–APV and 10 μM (+)MK801, were added to the bath with CPA in the pipette. For comparison, the time course for reduction in input resistance with 10 min treatment of 20 μM CPA in the bath (as in Fig. 2) is also provided (Black). Given that the experiments performed with CPA in the pipette (both red and green traces) do not have it in the bath, gray patch represents CPA treatment period only for experiments with CPA in the bath (only the black trace). (D–E) In experiments performed with CPA in the pipette, there was no significant difference in firing rate from the beginning of the experiment to a time point that is 45 min later. This was the case irrespective of whether there were NMDAR blockers in the bath (E) or not (D). (F) Population plots of f_R measured at the beginning of the experiment (Baseline; open circles) and 45 mins later (CPA; solid circles) showing significant increases (paired *Student's t* test) in experiments performed with standard ACSF in the bath (red), and with NMDAR blockers (green). (G) Time courses of normalized f_R in experiments performed with CPA in the recording pipette showed significant increases (red) in

resonance frequency 45 mins after the beginning of the experiment. The amount of increase was not significantly different even when NMDAR blockers (green), 50 μM D,L–APV and 10 μM (+)MK801, were added to the bath with CPA in the pipette. For comparison, the time course for increase in resonance frequency with 10 min treatment of 20 μM CPA in the bath (as in Fig. 1&2) is also provided (Black). Given that the experiments performed with CPA in the pipette (both red and green traces) do not have it in the bath, gray patch represents CPA treatment period only for experiments with CPA in the bath (only the black trace). (H) Relationship between changes in f_R and $\overline{R}_{in}$ during the experimental period establish the correlations between these two measurements for each of the three groups. (I) Summary plot of percentage changes in various measurements sensitive to the *h* current, at 40 mins after CPA wash in (for black boxes), or 45 min after the beginning of the experiment with CPA in the recording pipette (red and green boxes) relative to respective baseline values for each of the three groups. None of the measurements were significantly different between the groups where CPA was in the recording pipette and either standard ACSF (red) or NMDAR blockers (green) were in the bath. None of the measurements between the groups where CPA in the bath (black) and CPA in the recording pipette (red) were significantly different (*Mann-Whitney test*).

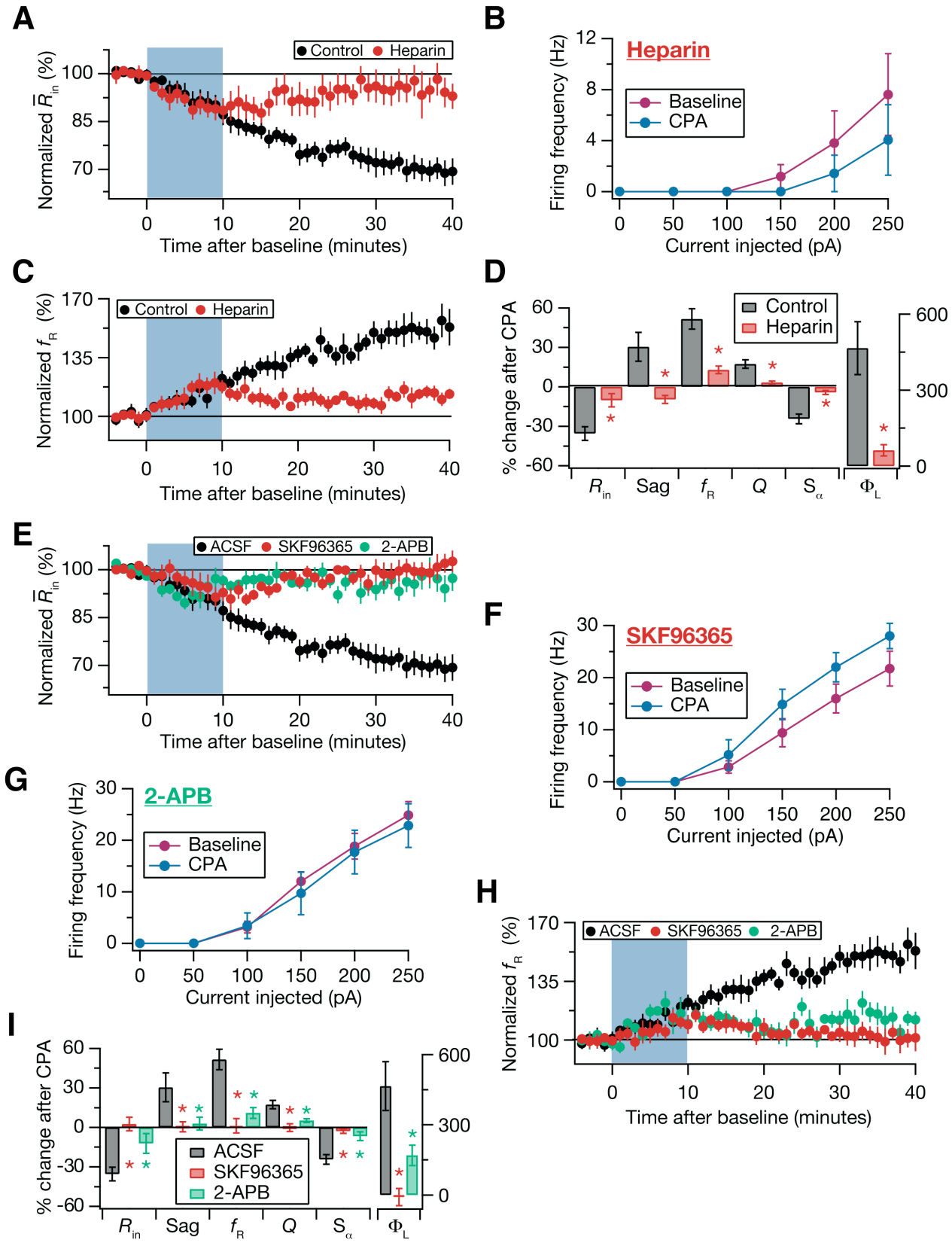
A
Control
Heparin
Normalized $\bar{R}_{in}$ (%)
100
85
70
0
10
20
30
40
Time after baseline (minutes)
B
Heparin
Baseline
CPA
Firing frequency (Hz)
12
8
4
0
0
50
100
150
200
250
Current injected (pA)
C
Control
Heparin
Normalized f_R (%)
170
135
100
0
10
20
30
40
Time after baseline (minutes)
D
Control
Heparin
% change after CPA
60
30
0
-30
-60
600
300
0
R_{in}
Sag
f_R
Q
S_α
Φ_L
E
ACSF
SKF96365
2-APB
Normalized $\bar{R}_{in}$ (%)
100
85
70
0
10
20
30
40
Time after baseline (minutes)
F
SKF96365
Baseline
CPA
Firing frequency (Hz)
30
20
10
0
0
50
100
150
200
250
Current injected (pA)
G
2-APB
Baseline
CPA
Firing frequency (Hz)
30
20
10
0
0
50
100
150
200
250
Current injected (pA)
H
ACSF
SKF96365
2-APB
Normalized f_R (%)
170
135
100
0
10
20
30
40
Time after baseline (minutes)
I
% change after CPA
60
30
0
-30
-60
600
300
0
ACSF
SKF96365
2-APB
R_{in}
Sag
f_R
Q
S_α
Φ_L

Figure S7. Depletion-induced plasticity in intrinsic excitability and resonance were dependent on inositol triphosphase ($InsP_3$) receptors and store-operated calcium (SOC) channels. Voltage recordings at the soma (V_m) were performed with 1 mg/mL of $InsP_3$ receptor blocker Heparin (N=6) in the pipette or with either 30 μM SKF96365 (N=6) or 50 μM 2-APB (N=5) in the recording solution. Blue patches represents CPA treatment period. Either drug (SKF96365 or 2-APB) was applied only for a few mins before and during the application of CPA. (A) In experiments performed with Heparin in the pipette (red), time courses of normalized $\overline{R}_{in}$ showed no significant change at 40 mins following CPA wash in. (B) Population plots of action potential firing frequency as a function of injected current to the soma establish the absence of any significant change (paired *Student's t* test) at 40 mins after CPA wash in (Baseline: magenta; 40 min after CPA: cyan). (C) In experiments performed with Heparin in the pipette (red), time courses of normalized f_R showed a significant increase at 40 mins following CPA wash in. (D) Summary plot of percentage changes in various measurements sensitive to the *h* current, at 40 mins after CPA wash in, relative to respective baseline values. Within the Heparin group, none of the measurements other than f_R (E) changed significantly after CPA treatment ($p>0.05$; paired *Student's t* test). However, across groups, percentage changes of all measurements in the Heparin group were significantly lesser (*: $p<0.05$; *Mann-Whitney* test) than those in the Control group. (E) In experiments performed with either SKF96365 (red) or 2-APB (green) in the recording solution, time courses of normalized $\overline{R}_{in}$ showed no significant change at 40 mins following CPA wash in. (F)–(G) In experiments performed either with SKF96365 (F) or 2-APB (G), population plots of action potential firing frequency as a function of injected current to the soma establish the absence of any significant change (paired *Student's t* test) at 40 mins after CPA wash in (Baseline: magenta; 40 min after CPA: cyan). (H) In experiments performed with either SKF96365 (red) or 2-APB (green) in the recording solution, time courses of normalized f_R showed no significant change at 40 mins following CPA wash in. In all the time courses of figure (parameters A, C, E and H), a transient change in the values of the parameters may be noticed immediately following CPA treatment. This change, although small, was significantly different from the baseline value in each of these cases. (I) Summary plot of percentage changes in various measurements sensitive to the *h* current, at 40 mins after CPA wash in, relative to respective baseline values. Within the SKF96365 and 2-APB groups, none of the measurements changed significantly after CPA treatment ($p>0.05$; paired *Student's t* test). Across groups, percentage changes of all measurements in the either the SKF96365 or the 2-APB groups were significantly lesser (*: $p<0.05$; *Mann-Whitney* test) than those in the Control group.

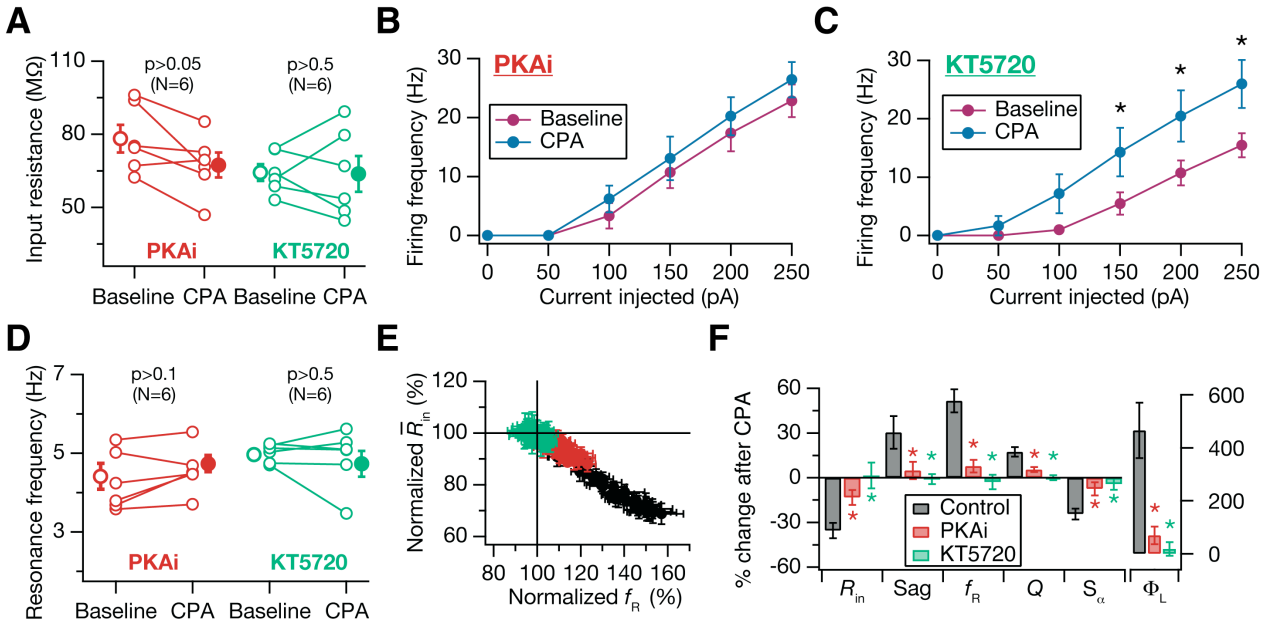

Figure S8. Depletion-induced plasticity in intrinsic excitability and resonance were dependent on the protein kinase A (PKA) pathway. Voltage recordings at the soma (V_m) were performed with either 20 μM PKA inhibitor peptide fragment (PKAi) in the pipette or 500 nM KT5720 in the recording solution. Application of KT5720 was preceded by a 30–45 min incubation of the slice in the KT5720. (A) In experiments performed in the presence of either PKAi or KT5720, population plots of R_{in} measured before (Baseline; open circles) and 40 mins after CPA wash in (CPA; solid circles) showed no significant changes (paired *Student's t* test) in R_{in}. (B)–(C) In experiments performed either with PKAi (B) or KT5720 (C), population plots of action potential firing frequency as a function of injected current to the soma establish no significant reductions ($p>0.1$; paired *Student's t* test) at 40 mins after CPA wash in (Baseline: magenta; 40 min after CPA: cyan). (D) In experiments performed in the presence of either PKAi or KT5720, population plots of f_R measured before (Baseline; open circles) and 40 mins after CPA wash in (CPA; solid circles) showed no significant changes (paired *Student's t* test). (E) Relationship between changes in f_R and $\overline{R}_{in}$ during CPA treatment experiments establish the correlations between these two measurements for each of the three groups. (F) Summary plot of percentage changes in various measurements sensitive to the *h* current, at 40 mins after CPA wash in, relative to respective baseline values. Within the PKAi (red) or KT5720 (green) groups, none of the measurements changed significantly after CPA treatment ($p>0.1$; paired *Student's t* test). Across groups, percentage changes of all measurements in the either the PKAi or the KT5720 group were significantly lesser (*: $p<0.05$; *Mann-Whitney* test) than those in the Control group.

Supplemental Experimental Procedures

Electrophysiology. Near-horizontal 350 μm hippocampal slices were prepared from 4–9 weeks old male Sprague Dawley rats using standard procedures(Narayanan and Johnston, 2008). The standard extracellular recording solution contained (in mM) 125 NaCl, 3 KCl, 1.25 NaH_2PO_4, 25 $NaHCO_3$, 2 $CaCl_2$, 1 $MgCl_2$ and 10 dextrose. Slices were incubated, for at least an hour, in a similar solution, but contained 2.5 mM KCl and 2 mM $MgCl_2$, in addition to 3 mM sodium pyruvate and 1.3 mM ascorbic acid. The whole-cell recording pipette solution contained (in mM) 120 K–gluconate, 20 KCl, 10 HEPES, 4 NaCl, 4 MgATP, 0.3 NaGTP, 7 K_2–phosphocreatine (pH 7.3 with KOH). For experiments with 20 mM K_4–BAPTA in the recording pipette solution, the amount of K–gluconate was reduced to 40 mM and the osmolarity was adjusted using sucrose (pH 7.3 with KOH). Neurons were visualized with differential interference contrast (DIC) microscopy using a Zeiss Axioskop microscope, fitted with a 60X (Olympus) water-immersion objective. Whole-cell patch recordings in current-clamp mode were made from the soma or the dendrites of CA1 pyramidal neurons using a Dagan IX2-700 amplifier. Signals were filtered at 5 kHz and sampled at 10–50 kHz. Recordings were made at 33–35° C. Electrodes were pulled from borosilicate glass, and their resistance was 4–6 MΩ for somatic recordings and 5–7 MΩ for dendritic recordings. During the course of the experiments, an estimate of the neuron's input resistance (denoted by $\overline{R}_{in}$) was measured from the steady state response of the cell to a 100 pA hyperpolarizing current pulse, which also was used to monitor and compensate, if necessary, for changes in series resistance. Experiments were discarded if, at any time during the course of the experiment, the access resistance crossed 25 MΩ for somatic recordings, or 40 MΩ for dendritic recordings. Data acquisition and analysis were performed with custom-written software in the *Igor Pro* environment (Wavemetrics Inc., USA).

Measurements. Input resistance (R_{in}) was measured as the slope of a linear fit to the steady state *V–I* plot obtained by injecting subthreshold current pulses of amplitudes spanning –50 pA to 50 pA, in steps of 10 pA (note that this is different from $\overline{R}_{in}$, above). Stimulus used for characterizing impedance parameters was a sinusoidal current of constant amplitude, a *Chirp* stimulus, with its frequency linearly spanning 0–15 Hz in 15 s (*Chirp15*; Fig. 4a). The magnitude and phase of the ratio between the Fourier transform of the voltage response and the Fourier transform of the *Chirp* stimulus formed the impedance amplitude and phase profiles, respectively. The frequency at which the impedance amplitude reached its maximum was the resonance frequency (f_R). Resonance strength (*Q*) was measured as the ratio of the maximum impedance amplitude ($|Z|_{max}$) to the impedance amplitude at 0.5 Hz. Total inductive phase (Φ_L) was measured as the area under the positive segment of the impedance phase profile (Narayanan and Johnston, 2007, 2008). The amplitude of the *Chirp15* stimulus was held constant (100 pA, peak-to-peak) through the course of the experiment. Percentage sag (*Sag*) was measured from the voltage response of the cell to a hyperpolarizing current pulse of 100 pA, and was defined as $100*(1-V_{ss}/V_{peak})$, where V_{ss} was the steady-state voltage deflection from baseline and V_{peak} was the peak voltage deflection from baseline. α-EPSPs were evoked by a current injections of the form $I_\alpha = I_{max}\, t \exp(-\alpha t)$, with $\alpha = 0.1$ /ms. Temporal summation ratio (S_α) in a train of 5 α-EPSPs at 20 Hz was computed as

E_{last}/E_{first}, where E_{last} and E_{first} were the amplitudes of last and first α-EPSPs in the train, respectively. In measuring temporal summation, the amplitude of a single EPSP was set the same (around 4–5 mV) before and after CPA treatment. This was done by changing I_{max}, and was necessary because of changes in input resistance after CPA treatment (Fig. 1–2). Voltages have not been corrected for the liquid junction potential, which was experimentally measured to be ~8 mV.

Drugs and chemicals. Most extracellular solution salts were procured from Fisher. $CaCl_2$, $NiCl_2$, K–Gluconate, MgATP, NaGTP, BAPTA, sucrose, ascorbic acid, and sodium pyruvate were from Sigma. Heparin, HEPES, and K_2Phosphocreatine were from EMD biosciences. Nimodipine, CGP55845, CPA, Tg, SKF96365, KN62, KN93, PKAi, KT5720, Ro 20-1724, cycloheximide and 2-APB were from Tocris. D,L–APV, (+)MK801, DNQX, (+)Bicuculline, Picrotoxin, TTX, and ZD7288 were from Ascent scientific. Experiments with any of the kinase inhibitors or cycloheximide involved pretreatment of the slice with the inhibitor for around 30–45 mins, followed by the presence of the inhibitor in the recording solution. Necessary care was taken, and appropriate controls were performed for each of the drugs used in order to make sure that there was no time dependent changes initiated by just the presence of the drug in the bath or in the pipette.

CPA/Tg treatment. Unless otherwise stated, the experimental protocol for all the experiments (Fig. 1B, bottom) involved an establishment of a five-min stable baseline of f_R and $\overline{R}_{in}$ (both measured from the *Chirp15* stimulus), following an initial measurement of α-EPSP summation, *V–I* (voltage vs. current plot to measure R_{in}) and *f–I* (action potential frequency as a function of depolarizing current injections) curves. Store depletion was induced using treatment with either cyclopiazonic acid (CPA) or thapsigargin (Tg) for 10 mins. Responses to the *Chirp15* stimulus were measured, twice every min, for 40 mins after the onset of drug washin, followed by a final measurement of α-EPSP summation, and the *V–I* and *f–I* curves. Unless otherwise stated, recordings were carried out at the initial resting membrane potential through the course of the experiment.

Cell-attached recordings. Somatic and dendritic I_h were measured in CA1 pyramidal neurons from acute hippocampal slices in the cell-attached patch clamp method using an Axopatch 200B amplifier (Molecular Devices Inc., CA). Slices were bathed in ACSF as indicated above, and cell-attached patches were formed using the following extracellular (pipette) solution (in mM): 100 KCl, 20 NaCl, 20 TEA-Cl, 10 HEPES, 5 EGTA, 5 4-AP, 1 $MgCl_2$, 3 $BaCl_2$, 1 $NiCl_2$, 0.5 $CdCl_2$, and 0.001 TTX, brought to a pH of 7.4 with TEA-OH. In experiments involving the application of CPA (or DMSO), seals were formed 30-60 minutes following the introduction of CPA (or DMSO) through the bath. I_h was elicited by 500 ms step hyperpolarizations from a holding potential that was 20 mV more positive than resting membrane potential (RMP) in –20 mV increments ranging from +10 to –90 mV (relative to RMP). Current recordings were filtered at 2 kHz and sampled at 10 kHz. Passive leak and capacitive transients were subtracted off-line using a scaled leak trace elicited by 10 mV depolarizations from the holding potential. Typically, between 100 and 220 individual leak traces were averaged in order to minimize the addition of noise to the leak subtracted current waveforms. Only

experiments with a maximal conductance greater than 8 pS and an obviously sigmoidal *g-V* relationship were included in our analysis. Currents from control experiments where 5 mM Cs^+ was added to the external (pipette) solution to block I_h never met these criteria. Although the resting membrane potential was determined in each experiment by breaking in, all reported voltages were standardized to the resting membrane potential determined from stable whole-cell current clamp recordings (using the previously described ACSF and internal solutions). These values were –62 mV (ACSF) and –59 mV (CPA), and were corrected for a measured liquid junction potential of +8 mV. Membrane potentials were additionally adjusted by -1 mV in order to correct for the liquid junction potential measured between the external (pipette) solution and the ACSF. The surface area of free membrane within the pipette was determined for each patch as described in (Sakmann and Neher, 1995). Conductance values were calculated using the experimentally determined reversal potential of –2 mV. Steady state *g-V* relationships were described using a Boltzmann function:

$$g(V) = g_{\max}\left(1+\exp\left(\left(V - V_{1/2}\right)/k\right)\right)^{-1}, \qquad (1)$$

where g_{max} is the maximum conductance, $V_{1/2}$ is the half maximal activation voltage, and k is the slope factor. Data acquisition was performed using Axograph X software (Axograph, Canberra, Australia), whereas data analysis and graphical displays were accomplished using IGOR Pro software (IGOR Pro, Lake Oswego, Oregon). All experiments were performed at 32–34° C, and all data points are displayed as mean ± SEM.

Data analysis. Unless otherwise stated, baseline values of f_R, *Sag*, Φ_L and *Q* were obtained by averaging measurements over the entire five min baseline period, and post-plasticity values were obtained by averaging measurements from the 35–40 min period from the onset of drug washin. For time course plots (*e.g.* Fig. 2C), two successive measurements (of f_R or $\overline{R}_{in}$) were averaged to obtain a single data value for each min, and this value was divided by the average baseline value throughout to obtain the normalized time course. The number of experiments performed in each group is provided in respective figures or in their legends. Group data are expressed as mean ± SEM. Depending on the dataset, statistical significance was calculated using paired or unpaired *Student's t* tests, or the *Mann-Whitney* test, or the *Kruskal-Wallis* test. Correlation was assessed using the *Pearson's* correlation test.

Computer simulations. Simulations were performed using the NEURON simulation environment (Carnevale and Hines, 2006). Integration time step for all simulations was set at 25 μs. Temperature was set at 34º C. A chirp current stimulus (Fig. 1B) was injected to obtain measurements of f_R and $\overline{R}_{in}$ under various parametric variations. Cell *n123* (Fig. 8A) from the Duke-Southampton archive (http://neuron.duke.edu/cells/) was used for all simulations. Passive properties were set as in (Narayanan and Johnston, 2007; Poirazi et al., 2003). The kinetics of the only active mechanism in the model, the *h*-channel, were set in accordance with experimental measurements (Fig. S11B) from the CA1 pyramidal neuron (Magee, 1998; Poolos et al., 2002). Specifically, the current through the *h* channel, I_h, is modeled as:

$$I_{\mathrm{h}} = \bar{g}_h \, s\left(V_{\mathrm{m}}, t\right)\left(V_{\mathrm{m}} - E_{\mathrm{h}}\right) \qquad (2)$$

where $\bar{g}_h$ denotes maximal *h* conductance; V_{m} , the membrane voltage and E_{h}, the reversal potential for the *h* channel. $s(V_{\mathrm{m}}, t)$ controls the voltage dependence and kinetics of the *h* channel, and evolves based on first-order kinetics (Gasparini *et al.*, 2004):

$$\frac{ds}{dt} = \frac{s_\infty - s}{\tau_h} \qquad (3)$$

$$s_\infty(V) = \left(1 + \exp\left(\left(V - V_{1/2}\right)/8\right)\right)^{-1} \qquad (4)$$

$$\tau_{\mathrm{h}}(V) = \frac{\exp(0.033(V + 75))}{0.011(1 + \exp(0.083(V + 75))} \qquad (5)$$

To match with experiments (Narayanan and Johnston, 2007), the distance-dependence of $\bar{g}_h$ as a function of distance from the soma (Lorincz et al., 2002; Magee, 1998) was set as a sigmoid

$$\bar{g}_h = 34\left(1 + \frac{100}{1 + \exp\left(\frac{380 - d_R}{34}\right)}\right) \mu\mathrm{S/cm}^2, \qquad (6)$$

where d_{R} corresponds to the radial distance (in μm) of the dendritic location from the soma (Narayanan and Johnston, 2007). Along the somato-apical trunk, $V_{1/2}$ was –82 mV for $d_{\mathrm{R}} \leq 100$ μm, linearly varied from –82 mV to –90 mV for $100 \leq d_{\mathrm{R}} \leq 300$ μm, and –90 mV for $d_{\mathrm{R}} > 300$ μm (Magee, 1998; Narayanan and Johnston, 2007). The basal dendrites had somatic $\bar{g}_h$ and $V_{1/2}$, and apical obliques had the same $\bar{g}_h$ and $V_{1/2}$ as the trunk compartment from which they originate (Poirazi et al., 2003). Unless otherwise stated, simulations were performed at –65 mV.

Supplemental References

Carnevale, N.T., and Hines, M.L. (2006). The NEURON Book (Cambridge University Press).

Gasparini, S., Migliore, M., and Magee, J.C. (2004). On the initiation and propagation of dendritic spikes in CA1 pyramidal neurons. J Neurosci *24*, 11046-11056.

Lorincz, A., Notomi, T., Tamas, G., Shigemoto, R., and Nusser, Z. (2002). Polarized and compartment-dependent distribution of HCN1 in pyramidal cell dendrites. Nat Neurosci *5*, 1185-1193.

Magee, J.C. (1998). Dendritic hyperpolarization-activated currents modify the integrative properties of hippocampal CA1 pyramidal neurons. J Neurosci *18*, 7613-7624.
Narayanan, R., and Johnston, D. (2007). Long-term potentiation in rat hippocampal neurons is accompanied by spatially widespread changes in intrinsic oscillatory dynamics and excitability. Neuron *56*, 1061-1075.
Narayanan, R., and Johnston, D. (2008). The h channel mediates location dependence and plasticity of intrinsic phase response in rat hippocampal neurons. J Neurosci *28*, 5846-5860.
Poirazi, P., Brannon, T., and Mel, B.W. (2003). Arithmetic of subthreshold synaptic summation in a model CA1 pyramidal cell. Neuron *37*, 977-987.
Poolos, N.P., Migliore, M., and Johnston, D. (2002). Pharmacological upregulation of h-channels reduces the excitability of pyramidal neuron dendrites. Nat Neurosci *5*, 767-774.
Sakmann, B., and Neher, E. (1995). Single-channel recording, 2 edn (New York: Plenum Press).